J Mater Sci: Mater Electron (2021) 32:6312–6322

Comparing low-temperature thermal and plasma sintering processes of a tailored silver particle-free ink

Wendong Yang[1,3,*], Felix Hermerschmidt[2], Florian Mathies[1], and Emil J. W. List-Kratochvil[1,2]

[1] Helmholtz-Zentrum Berlin Für Materialien Und Energie GmbH, Hahn-Meitner-Platz 1, 14109 Berlin, Germany
[2] Institut Für Physik, Institut Für Chemie, Humboldt-Universität Zu Berlin, IRIS Adlershof, Brook-Taylor-Straße 6, 12489 Berlin, Germany
[3] School of Electronic and Information Engineering, Liaoning Technical University, Huludao 125105, People's Republic of China

Received: 18 November 2020
Accepted: 15 January 2021
Published online: 5 February 2021

ABSTRACT

Silver particle-free inks are under rapid development due to their unique properties. Currently, most of the developed silver particle-free inks contain multiple components. In addition to the necessary solvents and silver precursors, these inks also contain complexing agents, reducing agents, and various additives. While such complex compositions assure good stability and printability of the inks, they hamper the sintering process as excess time and energy are often required to remove residues from various compositions to ensure high conductivities of the printed structures. Thus, a simple ink system is expected. On the other hand, plasma sintering shows its sintering potential in treating silver particle-free inks, but is only employed for the sintering of silver nitrate or silver acetate-based inks. Consequently, developing new particle-free ink systems with simple compositions and exploring the potential of plasma sintering is very meaningful. In this work, a clear and transparent silver particle-free ink was formulated, which can be treated both by low-pressure argon plasma sintering and low-temperature thermal sintering (120–160 °C). The roles of 2-amino-2-methyl-1-propanol (AMP) in the ink formulation were investigated in detail, which not only acts as the solvent but also as the complexing agent for silver oxalate to lower the sintering temperature of the ink. The electrical performance of the formulated ink was examined for both sintering processes for different conditions. The thermal sintering resulted in a resistivity value of 24.3 μΩ·cm on glass substrates after treatment at 160 °C for 60 min, while the plasma sintering yielded a resistivity value of 29 μΩ·cm at 500 W for 30 min. Compared to thermal sintering, plasma sintering achieved a similar electrical performance, but with a more nonuniform film structure. The power, sintering time, and the pressure of argon are key factors responsible for the conductivity of the produced films. Nevertheless, both resistivity values do meet the minimal electrical requirements of most electronic applications.

Address correspondence to E-mail: wendong_2007@163.com

https://doi.org/10.1007/s10854-021-05347-1

1 Introduction

The fabrication of good conductors on low-cost substrates has been the research focus of flexible electronics. Solution-based deposition processes, such as inkjet printing [1–4], gravure printing [5, 6], and slot die coating [7] show great potential in the scale and speed of producing such products, where a series of inks have been used [8]. Metal-particle-free inks, composed of metal salts or metal complexes and volatile solvents, are one of the representative ink materials which exist in the form of solution [9, 10]. This type of ink does not require stabilizers and usually has a lower sintering temperature and good stability (90–150 °C), showing its advantages over metal nanoparticle inks.

Silver particle-free inks have attracted great interest and are under rapid development [11–17]. Some of the developed silver particle-free inks have been used to fabricate highly conductive stretchable circuits [18], silicon solar cells [19], electrodes for organic field-effect transistors [20], and radiofrequency inductors [21]. Currently, most of the reported silver particle-free inks contain multiple components. In addition to the necessary solvents and silver precursors, these inks also contain reducing agents, complexing agents, and various additives [14, 15, 21]. Such a multi-component ink system presents some limitations: (1) more energy and time are required to remove various organic contents, and the inks need to be processed at high temperatures to achieve a good conductivity that precludes the use of many low-cost flexible substrates; (2) the additives used in the inks (e.g., organic binders) act as defects in the produced metallic film, lowering the conductivity. Since these additives remain in the final film, they also increase the sensitivity of the patterns to humidity and thereby reduce the reliability of the printed circuit; and (3) the utilization of reducing agent reduces the chemical stability of the ink over time. To overcome these issues, a simpler ink system with a reduced number of constituents is expected.

On the other hand, the post-treatment process at low temperature is desired for metal particle-free inks because this can broaden the range of flexible substrates. A post-treatment such as sintering is usually adopted for the ink patterns to acquire specific electronic properties [22]. This process brings thermal energy to the ink system so that the ink solvent can be evaporated and the silver ions are reduced to metallic silver. Up to now, various kinds of sintering methods have been reported [23] and each has its advantages and disadvantages. However, it should be noted that a faster sintering process without damaging thermally sensitive plastic substrates is always desired because this is conducive to the actual industrial manufacturing process.

Thermal sintering is the most commonly adopted technique for silver particle-free ink and is mostly carried out on a hotplate or in an oven. The required temperature varies from ink to ink depending on the composition of the ink. Thermal sintering can sinter the particles to form continuous features through Ostwald ripening [24]. For most common polymer flexible substrates, a low-temperature sintering is desired because they have a relatively low glass transition temperature.

Plasma sintering is also an attractive sintering method for silver conductive inks, which is carried out by exposure of printed patterns to low-pressure argon plasma [25, 26]. The exposure causes the evaporation or decomposition of the organic solvents and the reduction of silver ions within the printed feature from the top to the bottom. After a sufficient amount of sintering time, the as-printed features are converted into a continuous particle network. Plasma sintering has been employed to sinter silver nanoparticle inks [25–28].

Currently, for silver particle-free inks, efforts to achieve low-temperature sintering have focused on the careful design of the ink recipe [29]. A common and effective way is to use a weak reducing agent in ink formulation such as aldehyde-based materials (e.g., acetaldehyde, formic acid, dimethylformamide, glucose, and ethylene glycol) [30]. Apart from the modification of the ink recipe, the selection of advanced sintering techniques such as plasma sintering is also a suitable choice to decrease sintering temperature. Several works have been carried out. Bromberg et al. reported the application of argon plasma to convert printed lines of silver nitrate on glasses to silver traces [31]. The research showed that plasma sintering is a promising way for the rapid and low-temperature fabrication of metallization patterns. A patent from OrelTech Ltd also described the formation of the metal film with plasma treatment of a sliver nitrate ink in the concentration of 40 wt% in water [32]. In addition to silver nitrate ink, plasma

sintering of silver acetate ink has also been reported [24, 33]. These studies indicate the possibility of utilizing plasma to treat low-temperature silver particle-free inks. However, silver nitrate ink is not stable and explosive over time, and the synthetic methods for silver acetate inks are not economically feasible due to the utilization of highly toxic chemicals (e.g., ethylamine) and a longer aging time. Therefore, it is meaningful to exploit a new silver particle-free ink system and explore the sintering potential of plasma for flexible electronics.

In this contribution, we tailored a silver particle-free ink that is suitable for low-temperature treatment. The thermal and plasma sintering of the ink is presented. AMP, an alkanolamine, plays an important role in the ink recipe, which can not only serve as the solvent of the ink but also as the complexing agent for silver oxalate, leading to a very simple ink system that is suitable for low-temperature sintering. The electrical performance of the formulated ink was examined with thermal and plasma sintering, respectively. In terms of film microstructure, plasma sintering is not as good as thermal sintering. However, both sintering methods can achieve a resistivity in the order of 10^{-5} Ω·cm, which is in line with the targets required for electronic applications.

2 Experimental section

2.1 Chemicals

Silver nitrate ($AgNO_3$, ACS reagent, ≥ 99.0%), sodium hydroxide (NaOH, reagent grade, 97%, powder), oxalic acid ($H_2C_2O_4$, anhydrous, ≥ 99.0%) , and 2-amino-2-methyl-1-propanol ($C_4H_{11}NO$, AMP, for synthesis) were purchased from Sigma-Aldrich. Methanol (CH_4O, MA, gradient grade, ≥ 99.9%) was purchased from Honeywell. All chemicals were used as received without further purification. Glass substrates were used. Before ink deposition, 20 mm × 15 mm of glass sheets were ultrasonically cleaned in ethanol for 5 min to remove the particles and organic contaminations on the surface and then dried with a nitrogen gun. To obtain a hydrophilic surface for ink deposition, the substrates were further treated with a 5-min O_2-plasma process (Diener Femto PCCE plasma system, 0.35 mbar, 500 W, 40 kHz).

2.2 Ink formulation

The silver particle-free ink was formulated by simply dissolving the synthesized silver oxalate powder into alcohol solvents. The silver oxalate powder was prepared via an ion exchange method [34]. For ink preparation, 0.152 g of silver oxalate was first dispersed in 0.45 ml of methanol (MA). After stirring for 1 min, 0.3 ml of AMP was added. The mixture was further stirred for 60 min to produce a transparent ink. The solution was filtered through a 0.45 μm PTFE filter and directly used for the experiments.

2.3 Thermal and plasma sintering

The silver conductive films on pre-cleaned glass substrates were obtained by spin coating (3000 rpm, 30 s) with a subsequent thermal or plasma sintering process. 75 μl of the silver ink was used in a dynamic spin-coating process to obtain a thin layer that can cover the whole substrate. The thermal sintering was performed in air with a hotplate at 120 °C, 130 °C, 140 °C, 150 °C, 160 °C, and 170 °C for 5–60 min. The plasma sintering experiments were carried out with a plasma pencil using a low-pressure argon plasma instrument from Diener Electronic. Each plasma sintering experiment consisted of the following steps: (1) The chamber was evacuated to a pressure lower than 0.1 mbar; (2) argon gas was introduced into the chamber at a controlled flow rate (0.2 sccm) that was maintained for the duration of the experiment; and (3) after the flow rate and pressure stabilized, a plasma was initiated. Four power values (100, 250, 400 and 500 W) and five treatment times (5, 10,15, 20 and 30 min) were used for the experiments.

2.4 Characterization

Surface tension and contact angle of the formulated silver particle-free inks on glass substrates were measured with a drop-shaped analyzer (Krüss DSA100, Germany), using the pendant drop method and sessile drop method, respectively. The viscosity measurements were performed on a Haake rotational viscometer at 20 °C under 500 rpm. The thermal decomposition behaviors of the silver particle-free inks were investigated with a differential scanning calorimeter (Netzsch DSC 204 F1) and a thermogravimetric analyzer (Netzsch TG 209 F1). Measurements were carried out in the temperature range

30–300 °C with a heating rate of 10 °C min^{-1} under an argon atmosphere and a nitrogen atmosphere, respectively. The gas released from the thermogravimetric analyzer during the heating process was monitored with a coupled mass spectrometer (Netzsch QMS 403C). X-ray diffraction (XRD) analysis was carried out over a range of 20° to 90° on a Bruker D8 Advance X-ray diffractometer with a Cu Kα 1 radiation (λ = 0.15406 nm). The surface and cross-section morphologies of the obtained silver films were observed via a scanning electron microscope (HITACHI S-4100). Resistivity values were calculated via $\rho = R_s \times t$, where R_s and t are sheet resistance and the average thickness of the obtained silver films. R_s was measured on a four-point probe instrument (Jandel Engineering), and t was measured from the cross-section image.

3 Results and discussion

3.1 Ink formulation: roles of AMP

In this work, silver oxalate was chosen as the silver precursor of the ink because it has a higher silver content (71 wt%) than most of the organic silver precursors such as silver acetate and can be thermally reduced to metallic silver at low thermal decomposition temperatures (less than 200 °C) without organic residues [17, 34]. Methanol, a volatile and reducible alcohol, was used as the ink solvent to adjust the rheological properties as it has lower surface tension and viscosity than other alcohols such as ethanol and 2-propanol. AMP, an alkanolamine, was selected as the co-solvent of the ink due to its high viscosity (102 mPa·s, 30 °C, Fisher Scientific) and medium boiling point (165 °C).

The influences of the amount of AMP on the ink fluid and electrical properties were first investigated. Inks with different AMP content that are varied from 0.2 ml to 0.6 ml were formulated, as shown in Fig. 1a. When the content of AMP is below 0.2 ml, a transparent ink cannot be formulated. This means that the amount of AMP is not enough to completely react with the silver oxalate. And above this amount, a solution ink can be produced, mainly via the following complexing process (Fig. 1b). The lone pair of electrons on the nitrogen atom of AMP can coordinate with silver cations to produce a soluble silver-amine complex, thereby resulting in clear and transparent ink. FT-IR analysis was employed to confirm this process, as shown in Fig. 1c. The peaks associated with NH_2 groups of AMP undergo a dramatic red-shift after the reaction, implying that a coordination process occurred on the bond of NH_2. This phenomenon is similar to that of other silver-amine particle-free inks such as silver citrate-amine ink [35] and silver carbonate-amine ink [36].

The above results indicate that the AMP can not only act as the solvent in the ink but also as the complexing agent for silver oxalate. This is different from the common silver particle-free ink formula where a complexing agent is always necessary. In other words, our ink system is very simple, only consisting of a silver precursor and solvents.

The fluid properties such as surface tension, viscosity, and contact angle of each ink are given in Table 1; the corresponding images are given in Fig. S1 in the supporting information. As the content of AMP in the ink increases, the viscosity and surface tension of the ink increase gradually. SEM and four-point probe analyses were employed to investigate the morphology and resistivity differences of the film from each ink to determine the optimal content; the results are given in Fig. S2, where the AMP content has a significant influence on the resistivity of the film. As the AMP content increased from 0.3 to 0.6 ml, the resistivity of the film almost quadrupled. This can be easily understood. At high AMP content, the methanol content is relatively small, the ink viscosity is relatively large, the mass transfer is affected, and more organic residues are left, thereby making the conductivity poor. The corresponding SEM images indicate that the film obtained by the ink with 0.3 ml AMP was most compact and uniform. Therefore, this recipe was chosen for the following experiments, where the surface tension and viscosity of the ink were 25.86 mN/m and 6.64 mPa·s, respectively. These values are similar to those reported in our recent work about the printing research [37], which are within the range of fluid parameters required by a piezoelectric printer [4], indicating that the ink is printable. However, due to the lack of high-boiling-point solvents (T_b beyond 150 °C) in this ink formula, early drying and crystallization may appear when printing.

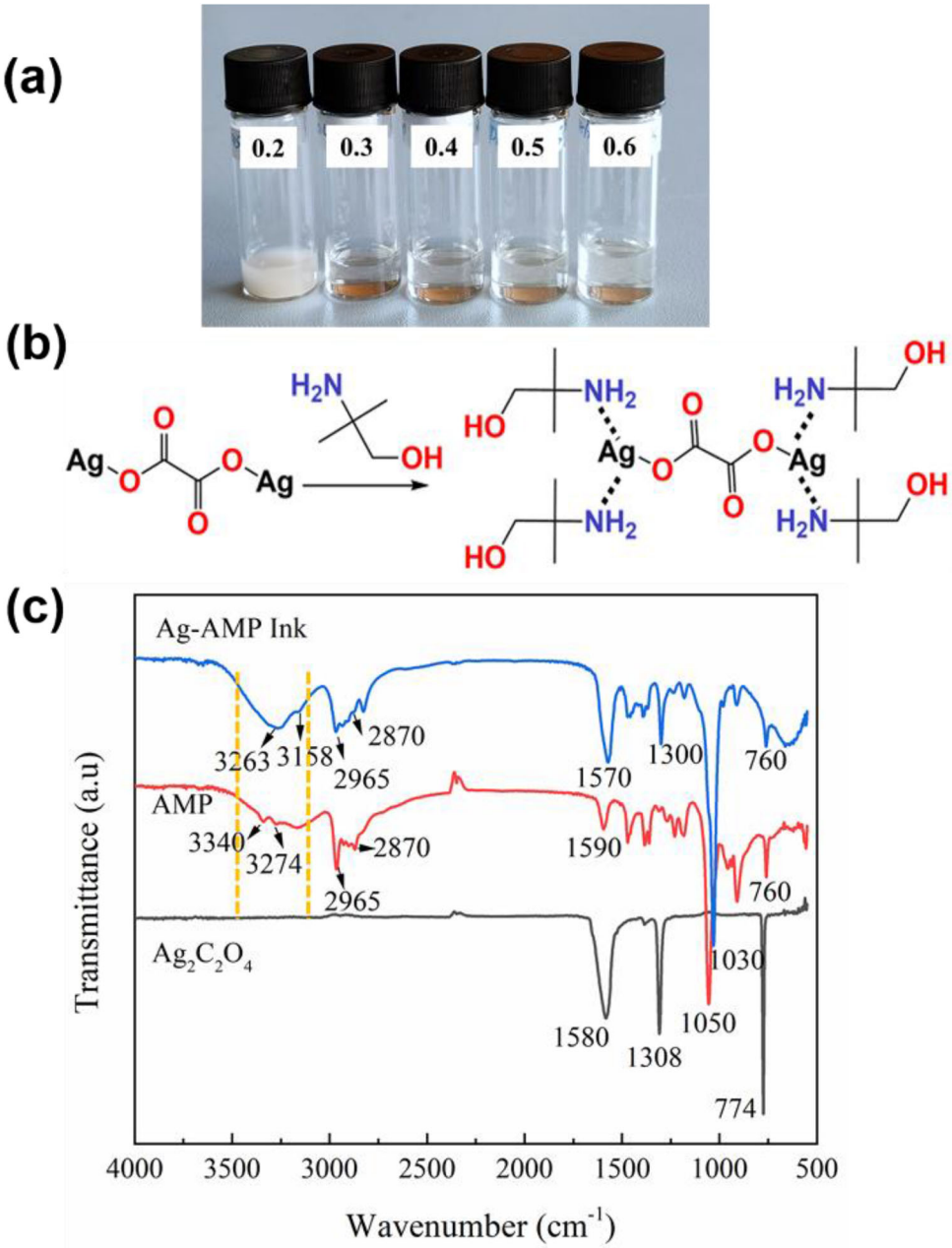

Fig. 1 **a** Image of inks with different AMP content varied from 0.2 to 0.6 ml, **b** the complexing mechanism of AMP and silver oxalate, and **c** FT-IR spectra of silver oxalate, AMP, and the Ag-AMP ink

Table 1 Fluid properties of the Ag-AMP inks with different AMP content

AMP content	0.3 ml	0.4 ml	0.5 ml	0.6 ml
Ink surface tension (γ, mN·m^{-1})	25.86	27.39	27.63	27.70
Ink viscosity (η, mPa·s, 20 °C)	6.64	7.31	8.71	9.78
Ink contact angle (glass substrate)	50.23°	53.6°	56.33°	56.67°

Ink recipe, 0.152 g silver oxalate, 0.45 ml MA, and 0.2–0.6 ml AMP

3.2 Thermal decomposition behavior of the ink

The thermal decomposition behavior of the optimal silver ink was investigated by DSC-TG-MS; the results are given in Fig. 2. The DSC curve shows three main endothermic peaks. The first two, around 75 °C and 130 °C, are attributed to the evaporation of the MA and the partial thermal reduction of Ag^{+}. This is in line with the results of MS (mass spectrometry) where MA and CO_2 gases were detected, respectively. The exothermic peak around 150 °C is from the decomposition of AMP [38]. The TG curve displays two main mass loss steps. The first step starts from 30 °C to 130 °C, corresponding to 40.2 wt% mass loss. The second step is between 130 and 180 °C, with a mass loss of 45.9 wt%. Thus, the final mass residue was 13.9 wt%, close to the theoretical silver content (13.2 wt%) of the ink. From the TG-DSC curve, it can be concluded that the decomposition temperature of the silver-amine complex in ink was about 130 °C, indicating the possibility of low-temperature sintering of conductive patterns. In combination with the decomposition temperature of silver oxalate (166–185 °C) [34], it can be concluded that AMP can lower the decomposition temperature of silver oxalate. This mild reducing ability may be related to the properties of the alkanolamine.

3.3 Film morphology

For silver particle-free ink, a post-treatment such as drying, curing, or sintering is required for the printed films or patterns to acquire specific electronic properties. Here, thermal sintering and plasma sintering were utilized for our ink system. An ink droplet of 75 µl was spin-coated on the glass substrates in order to achieve homogeneous thin films to assure reliable conductivity measurements. Silver films, obtained at various sintering parameters, were investigated by SEM and XRD to see the differences in the microstructure.

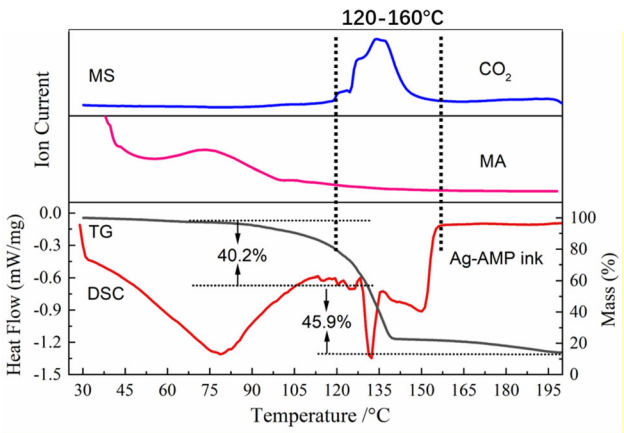

Fig. 2 Thermal decomposition behavior of the as-prepared Ag-AMP particle-free ink

Figure 3a shows the surface morphology of silver films sintered at 120 °C, 130 °C, 140 °C, 150 °C, 160 °C, and 170 °C for 60 min. All the films have a microstructure composed of interconnected domains of silver nanoparticles and few voids. This microstructural feature is a result of the fast evaporation of the solvent and thermal reduction of silver-AMP complex ions, where a lot of bubbles such as MA or CO_2 are produced and need to go through the films, thereby leaving a structure with pores. The film at 120 °C shows a compact microstructure consisting of small particles, mainly due to the insufficient decomposition and evaporation at this temperature. With further increasing the temperature, the size of the voids increased but the particle size became larger and most of them have a good connection with each other. Further increasing the sintering temperature to 170 °C, the microstructure development of silver films evolved to a stage dominated seemingly by the sintering of nanoparticles, as evidenced by such microstructural features as enlarged domain size and coalescence of pores. Here, the porosity and the average particle size of the films sintered at 130 °C, 150 °C and 170 °C were obtained using an image process technique [39] and Nanomeasre software. As the temperature increases, the porosity increases from 8.9% to 21.5%, and then 30.0%, while the average particle size increase from 99.2 to 133.8 nm, and then 206.1 nm. The average pore size for 170 °C is about 150 nm. These results indicate that the film is porous. According to reference [40] and [41], the silver porous nanostructures was an excellent substrate for chemical sensing using the SERS method. Therefore, our Ag porous nanostructures might be suitable for the SERS-related applications such as monitoring pesticide residues in agricultural products. Figure 3b gives the cross-section images of each film. The average thickness is about 300 ± 30 nm after sintering at a temperature above 150 °C for 60 min. The images also show that the film is made up of spherical interconnected silver nanoparticles.

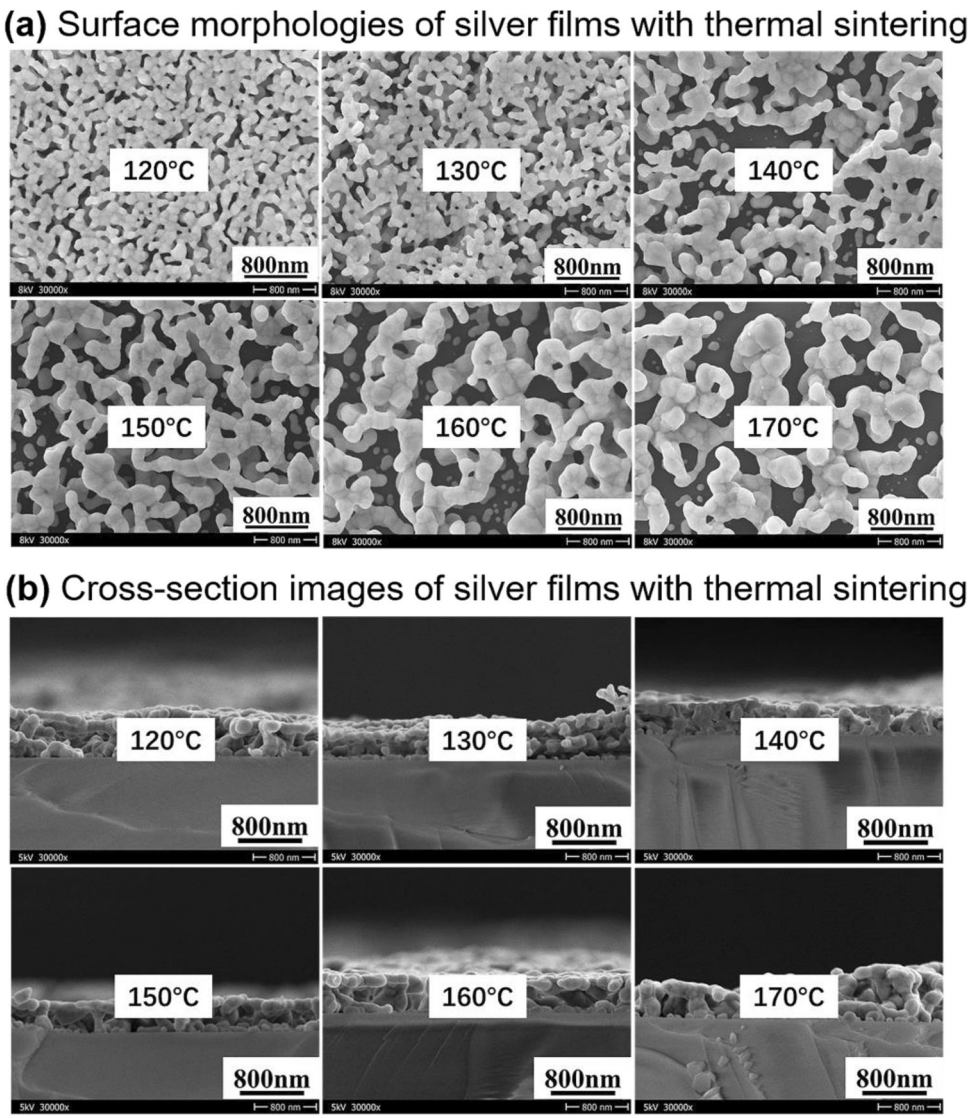

Fig. 3 Surface morphology (**a**) and cross-section (**b**) images of silver films sintered with a hot plate at 120 °C, 130 °C, 140 °C, 150 °C, 160 °C, and 170 °C for 60 min

Figure 4a shows the surface morphology of silver films sintered with low-pressure plasma, which is very different from the structure of the films with thermal sintering. The surface is composed of small-sized and multilayered silver nanoparticles and has many filamentous cracks. This structure is a result of the combined effects of plasma effect and rapid solvent evaporation. As the evaporation continues, the film will wrinkle and generate tensile stress. When the tensile stress exceeds the adhesion to the substrate, cracks will occur [42, 43]. However, the morphology of the crack is determined by many factors in the evaporation process, such as the characteristics of the substrate (wettability, roughness, etc.), and the evaporation rate, temperature, film thickness, etc. [44, 45]. These factors increase the difficulty of controlling film morphologies. Segmented sintering with different intensities of argon pressure may help to obtain a uniform film morphology, which can slow down the evaporation rate of the solvents and the decomposition of the silver-amine complex.

At 100 W of power, some small particles were generated on the surface of the glass substrates. These particles have an average size of 50 nm and most of them seem to be surrounded or wrapped by organic molecules. We suspect these small particles are the result of the thermal effect of the plasma [46], which will cause the evaporation of the ink solvents and the reduction of silver ions, thereby leading to the generation of silver particles. As power increases, the number of silver particles becomes more and more and the organic molecules decrease. Further

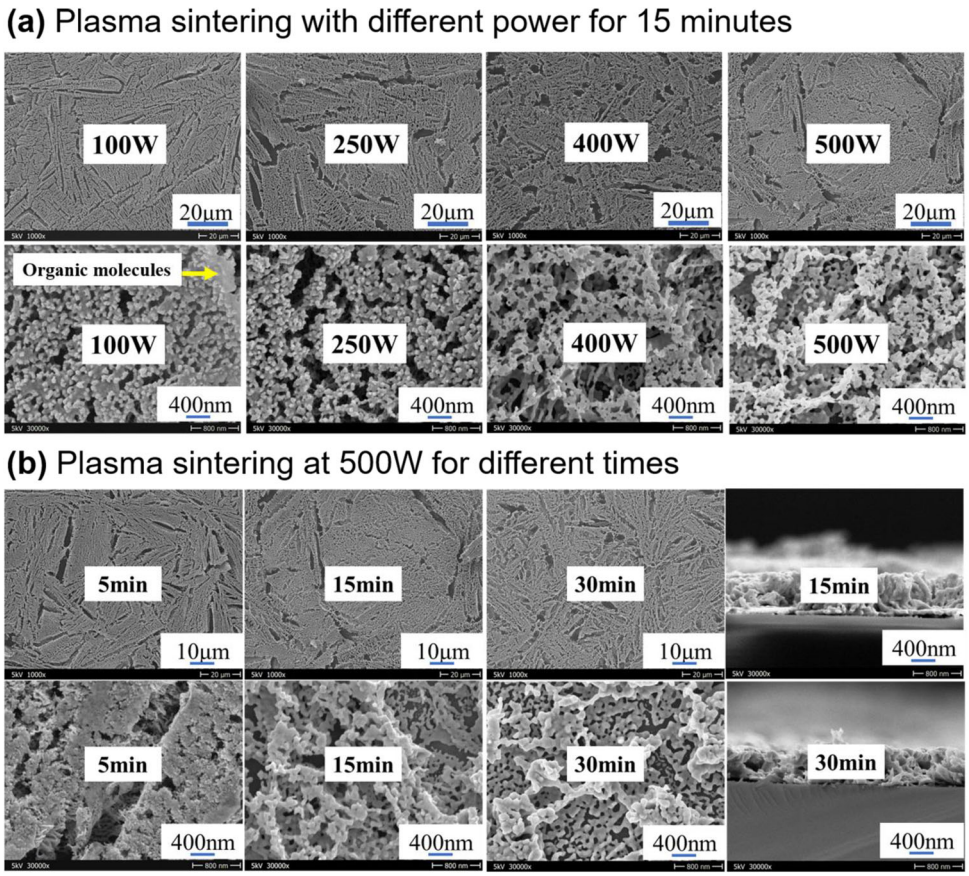

Fig. 4 **a** Surface morphologies of silver films sintered with plasma at different power for 15 min and **b** surface morphologies of silver films sintered with plasma at 500 W for different times

increasing the power of plasma to 500 W, the microstructure development of silver films evolved to a multilayer with few organic matters, where some of the interconnected silver particles are covered on the surface of others. This is attributed to another effect of plasma, the etching effect. The high energy and very active plasma particles break the chemical bonds in residual organic molecules [46] and remove them from the surface of the silver particles so that the particles have good contact. The produced silver nanoparticles merge and connect with adjacent particles, thereby resulting in a conductive network.

Figure 4b gives the morphologies and cross-section images of silver films sintered with plasma at 500 W (the maximum power of our instrument) for different lengths of time. The surface morphology gradually changes as time increases, evolving to a multilayer composed of interconnected silver particles. The average thickness is about 400 ± 30 nm after sintering at 500 W for 15–30 min. The images show that the film is made up of small silver nanoparticles stacked inline form. Here, it should be noted that the sintering of silver particle-free ink is very different from silver nanoparticle ink as the latter can be dried before sintering, that is why the treated films are not as good as reported in the literature in terms of microstructures.

X-ray diffraction was used to probe the crystalline structure of the silver films obtained with thermal sintering and plasma sintering, respectively; the results are given in Fig. S3. All the films show sharp distinct peaks corresponding to the characteristic values for metallic silver, revealing well-crystallized silver films. With the increase of sintering temperature or power, the intensity of diffraction peaks of silver films increases, meaning a better crystallinity.

3.4 Electrical performance

Figure 5 shows the resistivity of the silver films against sintering temperature or plasma power and time. For thermal sintering, the resistivity decreases close to a plateau value of 24.3 μΩ·cm with increasing sintering temperature to above 160 °C (Fig. 5a). At 120 °C, a resistivity below 10^{-5} Ω·cm has already been obtained. This value is higher than that of bulk silver

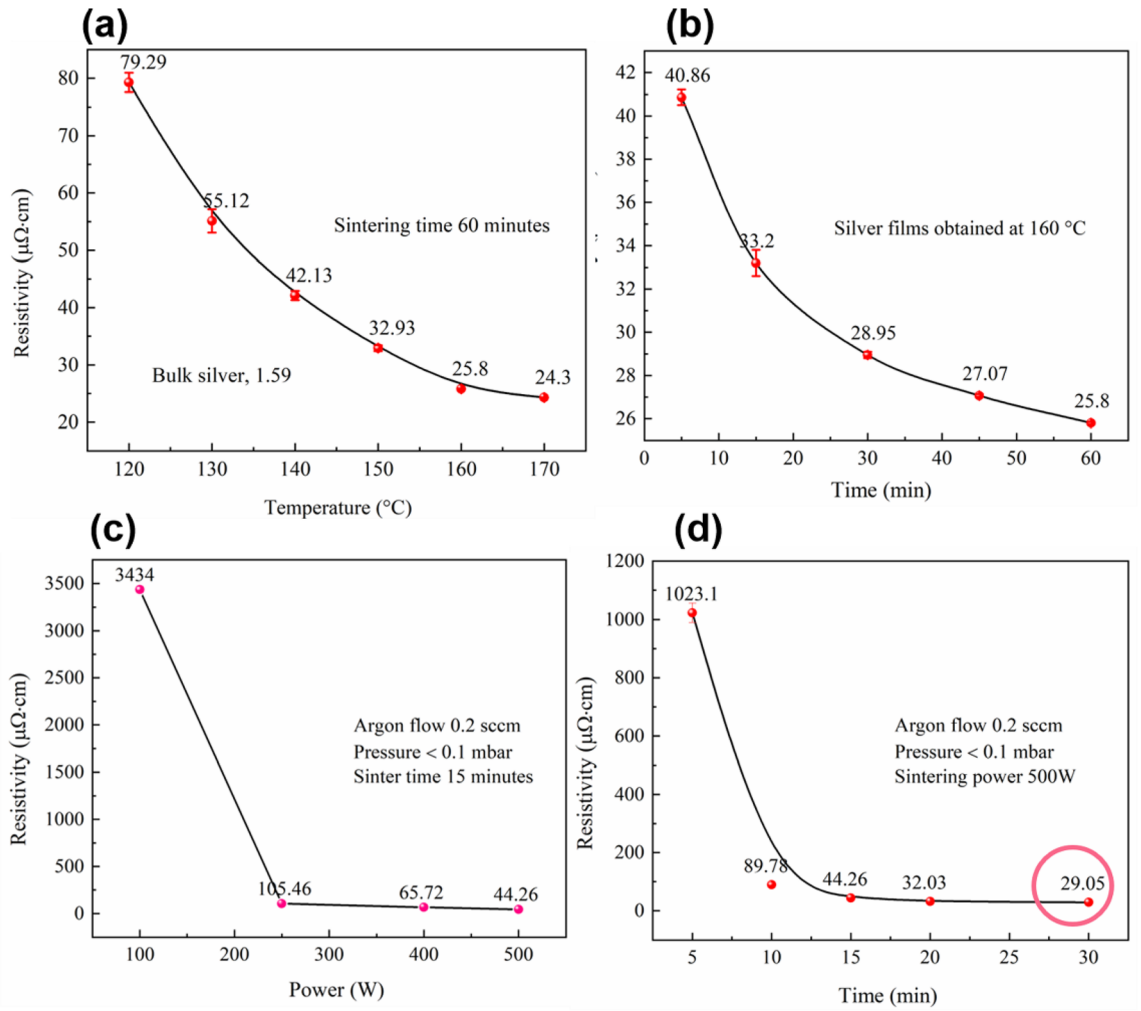

Fig. 5 **a** Resistivity of silver films sintered at different temperatures for 60 min and **b** at 160 °C for different times; **c** Resistivity of silver films sintered with plasma at different power for 15 min and **d** at 500 W for different times

and is associated with the reduction degree of silver-AMP complex ions and the residual degree of AMP that needs a temperature higher than that of 160 °C to remove. However, it can meet the electrical requirements of most electronic products. The changes in the resistivity with time are shown in Fig. 5b. After 5 min of sintering, the resistivity of the silver film is about 40 μΩ·cm, mainly due to the uncompleted reduction reaction. A significant decrease in resistivity was achieved by further increasing the sintering time to 30 min. After that, the resistivity decreases moderately and reaches 25 μΩ·cm at 60 min. For plasma sintering, the resistivity decreases significantly with the increase of plasma power (Fig. 5c) and time (Fig. 5d), reaching a value of 29 μΩ·cm at 500 W for 30 min. Further increasing the power could achieve a lower resistivity. However, this is limited by our available plasma instrument where the maximum power is 500 W.

Here, it is worth noting that the resistivity of the films sintered for 30 min by the two methods is almost the same. This means that the formation of a low resistivity film with plasma sintering of a silver particle-free ink is also possible, although the films from plasma sintering are not as uniform as the thermal sintering. Compared with thermal sintering, in terms of the control and adjustment of film microstructure, plasma sintering is more difficult due to the influences of many factors as previously mentioned. Here, we tried to slow down the drying rate of the ink by increasing the argon flow to 2 sccm in the chamber and the result shows insufficient sintering because a high resistivity was obtained.

Only under very low pressure can good electrical performance be achieved.

4 Conclusions

In summary, using an alkanolamine, AMP, as the complexing agent and solvent, transparent silver particle-free inks were formulated, which have a very simple two-component ink system and are suitable for low-temperature sintering. The effects of the amount of AMP on the fluid and electrical properties of the formulated inks were investigated, where an optimal ink was obtained. The ink with 13.68 Ag (wt%) was spin-coated on glass substrates and processed with thermal and plasma sintering, respectively. The former resulted in a resistivity value of 24.3 μΩ·cm on glass substrates after sintering at 160 °C for 60 min, while the latter yielded a resistivity value of 29.05 μΩ·cm at 500 W for 30 min. In comparison with thermal sintering, plasma sintering achieved a nonuniform film structure, but with similar electrical performance.The presented work shows that the careful design of the ink formula plays a decisive role in realizing low-temperature sintering. Further improvement on the ink properties such as electrical, thermal, and fluid properties could focus on the selection of silver carboxylates (unsaturated, branched, and/or substituted with a hydroxyl group) that are easy to be transformed into silver and alkanolamine possessing multiple silver binding sites and a boiling point below 150 °C. An additive-free ink that is well designed has good stability and can save energy and time in achieving good conductivity and film morphologies, and good adhesion still remains an issue to be addressed.

Acknowledgement

This work was carried out in the framework of the Joint Lab GEN_FAB. The authors acknowledge the funding by the German Federal Ministry of Education and Research (BMBF), the Helmholtz Energy Materials Foundry (HEMF), and PEROSEED (ZT-0024) project. The authors are also grateful to Claudia Leistner, Carola Klimm, and René Gunder for their assistance in the DSC-TG-MS, SEM, and XRD measurements, respectively.

Funding

Open Access funding enabled and organized by Projekt DEAL.

Compliance with ethical standards

Conflict of interest No conflict of interest exits in the submission of this manuscript and it is approved by all authors.

Supplementary Information: The online version of this article (https://doi.org/10.1007/s10854-021-05347-1) contains supplementary material, which is available to authorized users.

References

1. P. Calvert, Chem. Mater. **13**, 3299 (2001)
2. M. Singh, H.M. Haverinen, P. Dhagat, G.E. Jabbour, Adv. Mater. **22**, 673 (2010)
3. F. Hermerschmidt, S.A. Choulis, E.J. List-Kratochvil, Adv. Mater. Technol. **4**, 1800474 (2019)
4. F. Mathies, E.J. List-Kratochvil, E.L. Unger, Energy Technol. **8**, 1900991 (2020)
5. G. Hernandez-Sosa, N. Bornemann, I. Ringle, M. Agari, E. Dörsam, N. Mechau, U. Lemmer, Adv. Funct. Mater. **23**, 3164 (2013)
6. R. Kitsomboonloha, S. Morris, X. Rong, V. Subramanian, Langmuir **28**, 16711 (2012)
7. H. Lee, D. Lee, J. Hwang, D. Nam, C. Byeon, S.H. Ko, S. Lee, Opt. Express **22**, 8919 (2014)

8. L. Nayak, S. Mohanty, S.K. Nayak, A. Ramadoss, J. Mater. Chem. C **7**, 8771 (2019)
9. W. Yang, E.J.W. List-Kratochvil, C. Wang, J. Mater. Chem. C **7**, 15098 (2019)
10. Y. Choi, K.D. Seong, Y. Piao, Adv. Mater. Interfaces **6**, 1901002 (2019)
11. X. Nie, H. Wang, J. Zou, Appl. Surf. Sci. **261**, 554 (2012)
12. S.F. Jahn, T. Blaudeck, R.R. Baumann, A. Jakob, P. Ecorchard, T. Rüffer, H. Lang, P. Schmidt, Chem. Mater. **22**, 3067 (2010)
13. S.P. Chen, Z.K. Kao, J.L. Lin, Y.C. Liao, A.C.S. Appl, Mater. Interfaces **4**, 7063 (2012)
14. S.B. Walker, J.A. Lewis, J. Am. Chem. Soc. **134**, 1419 (2012)
15. K.S. Bhat, R. Ahmad, Y. Wang, Y.B. Hahn, J. Mater. Chem. C **4**, 8522 (2016)
16. Y. Dong, X.D. Li, S.H. Liu, Q. Zhu, J.G. Li, X.D. Sun, Thin Solid Films **589**, 381 (2015)
17. K.R. Zope, D. Cormier, S.A. Williams, A.C.S. Appl, Mater. Interfaces **10**, 3830 (2018)
18. M. Hu, X. Cai, Q. Guo, B. Bian, T. Zhang, J. Yang, ACS Nano **10**, 396 (2016)
19. Y. Tamari, A. Gautrein, C. Schmiga, S. Binder, M. Glatthaar, S.W. Glunz, Energy Procedia **55**, 708 (2014)
20. S. Gamerith, A. Klug, H. Scheiber, U. Scherf, E. Moderegger, E.J. List, Adv. Funct. Mater. **17**, 3111 (2007)
21. M. Vaseem, G. McKerricher, A. Shamim, A.C.S. Appl, Mater. Interfaces **8**, 177 (2016)
22. S. Wünscher, R. Abbel, J. Perelaer, U.S. Schubert, J. Mater. Chem. C **2**, 10232 (2014)
23. F. Hermerschmidt, D. Burmeister, G. Ligorio, S.M. Pozov, R. Ward, S.A. Choulis, E.J. List-Kratochvil, Adv. Mater. Technol. **3**, 1800146 (2018)
24. N. Wang, Y. Liu, W. Guo, C. Jin, L. Mei, P. Peng, Nanotechnology **31**, 305301 (2020)
25. S. Wünscher, S. Stumpf, A. Teichler, O. Pabst, J. Perelaer, E. Beckert, U.S. Schubert, J. Mater. Chem. C **22**, 24569 (2012)
26. I. Reinhold, C.E. Hendriks, R. Eckardt, J.M. Kranenburg, J. Perelaer, R.R. Baumann, U.S. Schubert, J. Mater. Chem **19**, 3384 (2009)
27. S. Ma, V. Bromberg, L. Liu, F.D. Egitto, P.R. Chiarot, T.J. Singler, Appl. Surf. Sci. **293**, 207 (2014)
28. F.M. Wolf, J. Perelaer, S. Stumpf, D. Bollen, F. Kriebel, U.S. Schubert, J. Mater. Res. **28**, 1254 (2013)
29. Y. Mou, Y. Zhang, H. Cheng, Y. Peng, M. Chen, Appl. Surf. Sci. **459**, 249 (2018)
30. Y. Tao, Y. Tao, B. Wang, L. Wang, Y. Tai, Nanoscale Res. Lett. **8**, 1 (2013)
31. V. Bromberg, S. Ma, F.D. Egitto, T.J. Singler, J. Mater. Chem. C. **1**, 6842 (2013)
32. N. Zamoshchik, U.S. Patent, Application No. 15/491,036., 2017.
33. C.E. Knapp, J.B. Chemin, S.P. Douglas, D.A. Ondo, J. Guillot, P. Choquet, N.D. Boscher, Adv. Mater. Technol. **3**, 1700326 (2018)
34. W. Yang, C. Wang, V. Arrighi, J. Electron. Mater. **47**, 2824 (2018)
35. J.J. Chen, G.Q. Lin, Y. Wang, E. Sowade, R.R. Baumann, Z.S. Feng, Appl. Surf. Sci. **396**, 202 (2017)
36. Y. Cai, X. Yao, X. Piao, Z. Zhang, E. Nie, Z. Sun, Chem. Phys. Lett. **737**, 136857 (2019)
37. W. Yang, F. Mathies, E. Unger, F. Hermerschmidt, E. List-Kratochvil, J. Mater. Chem. C **8**, 16443 (2020)
38. T. Wang, K.-J. Jens, Ind. Eng. Chem. Res. **51**, 6529 (2012)
39. M. Abbasgholipourghadim, M. Mailah, I. Z. M. Darus, A. F. Ismail, M. R. Dashtarzhandi, M. Abbasgholipourghadim and S. Khademi, Proceedings of the 6th International Conference on Fluid Mechanics and Heat Mass Transfer, 113 (2015).
40. R. Jiang, W. Xu, Y. Wang, S. Yu, New J. Chem **42**, 17750 (2018)
41. Z. Liu, L. Wang, W. Bian, M. Zhang, J. Zhan, RSC Adv. **7**, 3117 (2017)
42. C. Allain, L. Limat, Phys. Rev. Lett. **74**, 2981 (1995)
43. V. Lazarus, L. Pauchard, Soft Matter **7**, 2552 (2011)
44. W.P. Lee, A.F. Routh, Langmuir **20**, 9885 (2004)
45. K.B. Singh, M.S. Tirumkudulu, Phys. Rev. Lett. **98**, 218302 (2007)
46. J. Li, Y. Tao, S. Chen, H. Li, P. Chen, M.-Z. Wei, H. Wang, K. Li, M. Mazzeo, Y. Duan, Sci. Rep. **7**, 1 (2017)